

## CHAPTER 3

ANTIPROTON PRODUCTION3.1 Antiproton Yields and Targeting

The choice of the antiproton energy and that of the protons for their production depend on the production cross sections and practical considerations relative to the existing facilities at the Laboratory. This section describes the present targeting scenario for the production of antiprotons, based on the discussion of the three following topics:

1. details of the production cross sections obtained from existing experimental data;
2. the choice of primary proton energy, antiproton momentum, antiproton longitudinal acceptance and antiproton transverse acceptance; and
3. limitations introduced by targeting and the antiproton collection system.

3.1.1 Antiproton Production Cross Sections. The available experimental data on the cross sections for the production of antiprotons have been described by a phenomenological formula that includes the dependence on the incident proton energy, the antiproton momentum and the target nucleus.<sup>1</sup> For example, the yields of antiprotons from a tungsten target collected within a laboratory angle of 60 mrad for various proton energies are shown in Fig. 3-1. It can be seen that there is a plateau at 120 GeV for the production of antiprotons between 8 and 13 GeV/c.

3.1.2 Proton Energy. The yield of antiprotons per unit volume of phase space per unit time changes very slowly with proton energy above 150 GeV, when the Main Ring cycle time is taken into consideration. Although some gain in yield could be obtained by going to a higher energy, a proton energy of 120 GeV was chosen because it is the maximum energy that can be extracted from a medium straight section such as F17. F17 provides a convenient location for the Antiproton Source. The choice was also influenced by the rapid increase in operating cost as the energy of the Main Ring is increased. The energy of 120 GeV is also compatible with the Colliding Beams Detector overpass. The B0 overpass is described in Chapter 7.

3.1.3 Antiproton Momentum. The optimum antiproton momentum is 10.0 GeV/c for an incident proton energy of 120 GeV. The yield is more than 90% of the optimum yield throughout the range from 7.5 GeV/c to 13.0 GeV/c. Since the normal injection momentum of the Main Ring, 8.89 GeV/c, is within this range of momenta, it is a reasonable choice. It has the advantage of

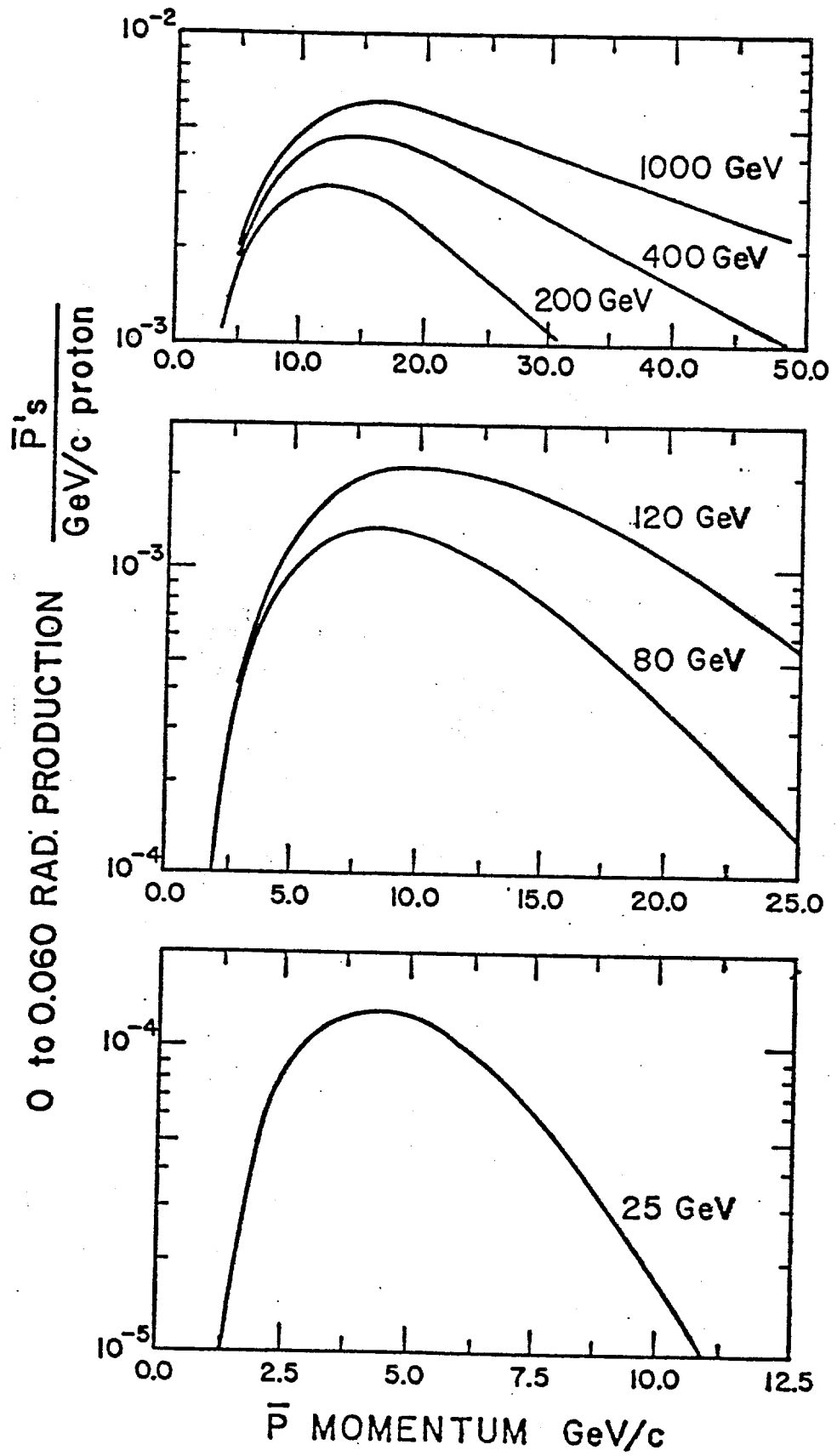


Figure 3-1

permitting the transfer of antiprotons directly from the Accumulator to the Main Ring. In addition, it opens the possibility of utilizing protons directly from the Booster as an alternative source of particles during commissioning of the source.

3.1.4 Antiproton Longitudinal Acceptance. Stochastic-cooling performance depends critically on the flux of p's injected into the Accumulator and on the particle density per unit of energy spread. This density, which is inversely proportional to the longitudinal emittance of the antiprotons, is determined in part by the time spread of the  $\bar{p}$ 's at production, as discussed in Chapter 2.

In the Debuncher, a total momentum spread of approximately 3% can be reduced to a momentum spread that can be accommodated by the Accumulator. Although a larger momentum spread will result in a larger flux the Accumulator is not able to cool the larger flux. The  $\bar{p}$  collection and transport system is designed to accept 4% total momentum spread. The momentum spread of the  $\bar{p}$ 's transported to the Debuncher will be adjusted by collimation in the beam transport.

3.1.5 Antiproton Transverse Acceptance. The calculation of expected antiproton yields depends crucially on the collection system downstream of the target. A comparison of different collection systems has been performed<sup>2</sup>, taking into account the large momentum spread of the antiproton beam. The advantages of a device such as the lithium lens that was developed at the INP in Novosibirsk<sup>3</sup> are clear. It has a very short focal length and it focuses in both transverse planes. Based on the INP experience, the parameters of the lithium lens collector were chosen to be: Radius = 1 cm, Gradient = 1000 T/m, Length = 15 cm. Within the present technology developed at Novosibirsk, a repetition rate of 1 Hz is feasible. The lens has a focal distance of 14.5 cm. The short focal distance requires the use of a dense target.

Antiprotons yields have been calculated with a Monte Carlo program<sup>1</sup> that includes the phenomenological description of the production cross section, the development of hadronic showers in the target and  $\bar{p}$  production by secondaries, multiple scattering and absorption. The result of these calculations is shown in Fig. 3-2 for two different rms proton beam spot sizes,  $\sigma_x = \sigma_y = 0.038$  cm and  $\sigma_x = \sigma_y = 0.22$  cm. The number of antiprotons increases<sup>x</sup> approximately linearly with the transverse acceptance above  $20\pi$  mm-mrad for  $\sigma = 0.038$  cm. For the smaller beam size, the departure from linearity above  $20\pi$  mm-mrad is caused by the finite lithium lens radius and the variation of field gradient. The optimum target length is approximately 5 cm.

3.1.6 Targeting Limitations. Decreasing the proton beam size at the target increases the transverse phase-space density of the produced

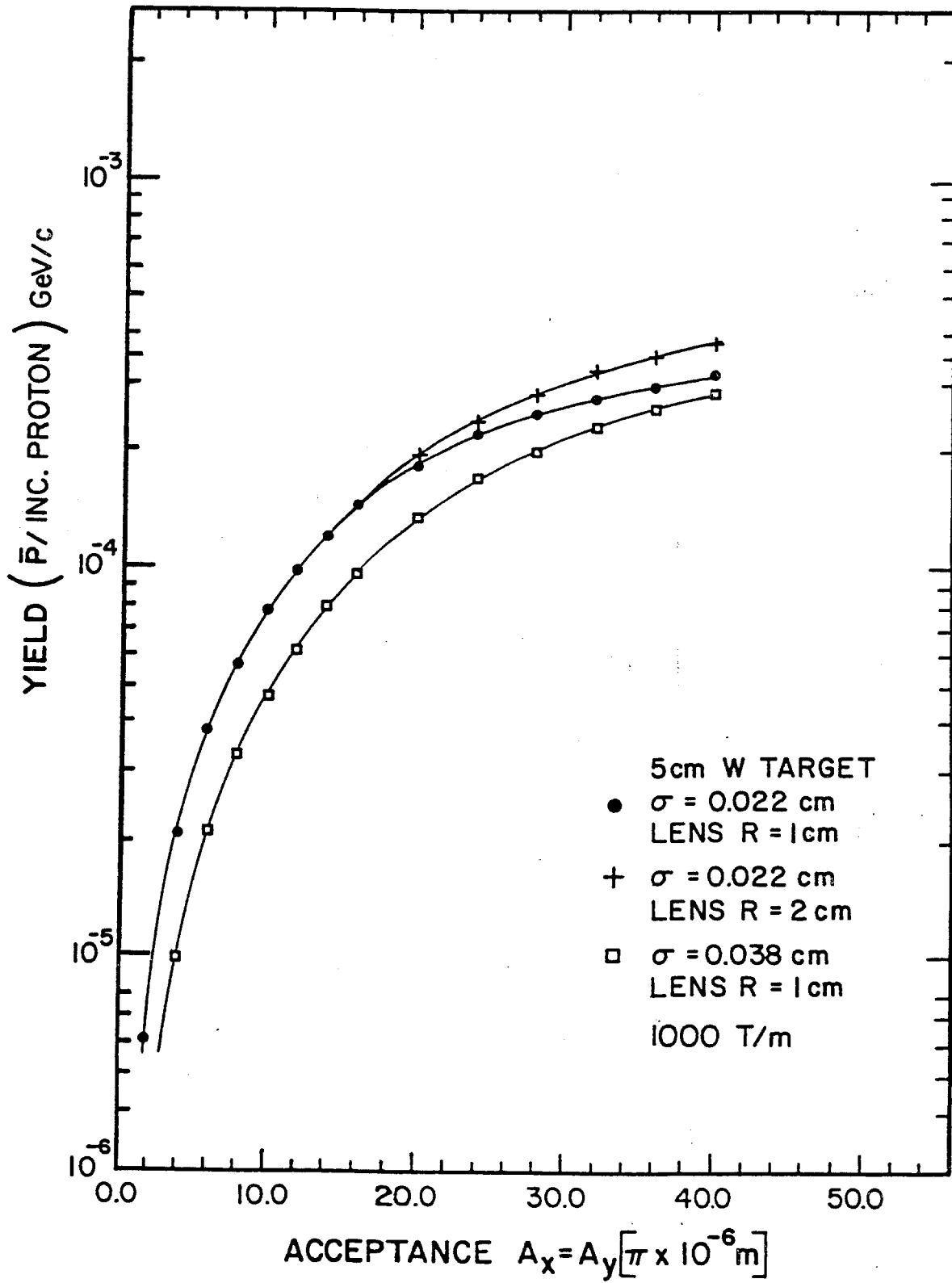


Figure 3-2

antiprotons, resulting in a larger yield within a given acceptance. The diameter of the proton beam cannot be reduced arbitrarily because the energy deposited by the beam per unit volume increases as the beam area decreases, causing the target to overheat.

The subject of high energy density deposition in targets was the subject of a Fermilab Workshop<sup>5</sup>. It was generally agreed that metal targets can sustain energy density deposition up to 200 Joules gm<sup>-1</sup> before the apparent onset of shock waves that could result in the destruction of the target. Calculations indicate that the CERN Antiproton Accumulator target sustains a maximum energy deposition of approximately 185 Joules/gm for tungsten. Both copper and rhenium (instead of tungsten) have been used at CERN for some time with no failures. The energy density deposited by a 120-GeV proton beam in tungsten has been calculated using the program MAXIM<sup>4</sup>. The maximum energy density deposited within a 5-cm long target is shown in Fig. 3-3 versus the rms size of the proton beam,  $\sigma$ . Within the errors of the calculation, it varies as  $\sigma^{-2}$ . Also shown is the maximum number of protons per pulse vs rms beam size, under the condition that the maximum allowable energy density is 200 Joules/gm.

Table 3-I shows the expected number of antiprotons per pulse as a function of beam size and maximum permissible proton intensity.

A feasibility study was carried out<sup>6</sup> on sweeping the proton beam across the target to decrease the energy density deposited in the material. The antiproton acceptance must be simultaneously swept to track the proton beam spot. If the sweeping covers several proton-beam diameters, it is possible to target  $3 \times 10^{12}$  protons on beam spots corresponding to  $\beta < 3$  m, which will give an increased number of antiprotons accepted per proton. The design of the target area makes it possible to incorporate a beam-sweeping system in the future.

TABLE 3-I NUMBER OF ANTIPROTONS PER PULSE

$\beta^*(m)^+$	$\sigma_x = \sigma_y$ (cm)	$N_p(\text{Max})$	$\bar{p}/p^{++}$	$\bar{p}/\text{pulse}$
1.55	0.023	$6.0 \times 10^{11}$	$5.1 \times 10^{-5}$	$3.1 \times 10^7$
3.07	0.032	$1.2 \times 10^{12}$	$4.3 \times 10^{-5}$	$5.2 \times 10^7$
4.62	0.039	$1.8 \times 10^{12}$	$3.7 \times 10^{-5}$	$6.7 \times 10^7$
8.00	0.052	$3.0 \times 10^{12}$	$2.5 \times 10^{-5}$	$7.5 \times 10^7$

Notes: +  $\beta^*$  is for the proton beam at the center of the target  
( $\beta = \beta_x = \beta_y = \beta^*$ )

++ The yield in  $\bar{p}/\text{proton}$  is for 3%  $\Delta p/p$  and  $20\pi$  mm-mrad.

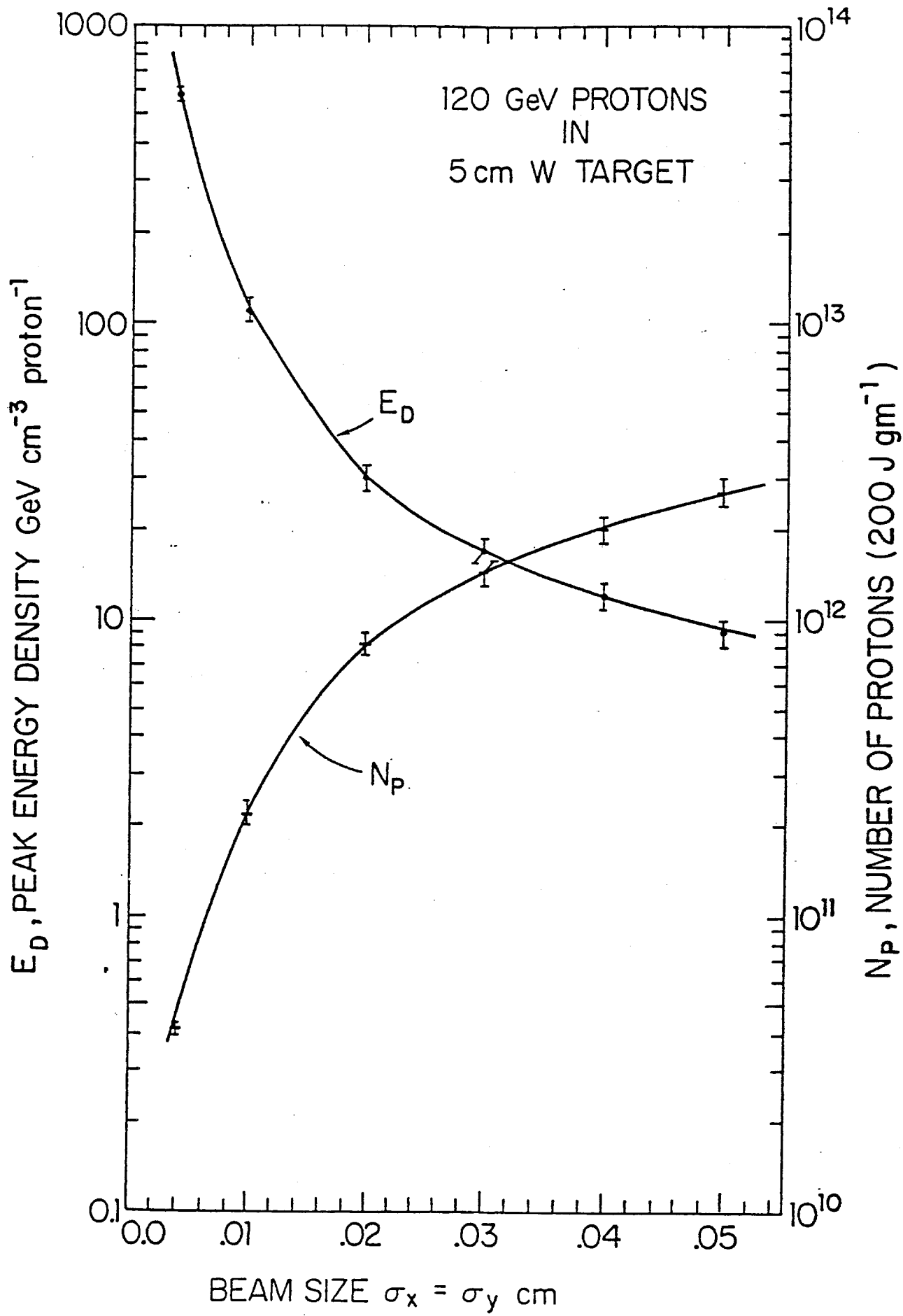


Figure 3-3

### 3.2 Antiproton Target System Components

The principal components of the target system are the target itself and the antiproton collection device. This section discusses the design and limitations of these two components.

3.2.1 Antiproton Production Target The computer code MAXIM<sup>4</sup> has been used to calculate radial and longitudinal energy density distributions in a stationary tungsten target for an rms beam size of 0.038 cm. The results are plotted in Fig. 3-4. The temperature rise of tungsten corresponding to an energy deposition in Joules/gm may be estimated from the enthalpy reserve curve given in Fig. 3-5. As is shown in Fig. 3-4, it is expected that local peak energy densities will be approximately 200 Joules/gm for the present design parameters  $\sigma = 0.038$  cm and  $2 \times 10^{12}$  protons per pulse. To decrease the number of thermal and stress cycles in the volume of material struck by the beam, the target will be rotated continuously, exposing a new volume of material to each beam pulse. Two possible configurations are shown in Figs. 3-6 and 3-7. During the target development stage the wedges shown in Fig. 3-6 will contain different materials to allow for comparative testing. Provision is also being made to test stationary targets of the CERN design.

The target must have a high density and high melting point. A compilation of mechanical properties for different materials was performed. A figure of merit to compare the mechanical properties is given by the yield stress divided by the coefficient of thermal expansion and the modulus of elasticity. On this basis rhenium, tungsten and tungsten-rhenium alloys are in increasing order for this figure of merit. The coefficient of heat conductivity could also be included in the figure of merit without significantly altering the choice of material.

The high-temperature behavior of tungsten-rhenium alloys shows considerable increase of yield stresses with respect to tungsten, but little change in the coefficient of thermal expansion or the modulus of elasticity. Tungsten-rhenium alloys are utilized in industry for high-temperature applications such as incandescent-lamp wire and targets for high-power x-ray tubes. A significant amount of experience with the technology for their fabrication exists. Tungsten has been used for all  $\bar{p}$  yield calculations, although a number of target configurations will be tested during the R & D phase of the target-station development. A summary of the target parameters is given in Table 3-II.

TABLE 3-II TARGET PARAMETERS

Target Material	Tungsten/Tungsten Alloys
Length	5 cm
120 GeV protons/pulse	$2.0 \times 10^{12}$
Total Beam Energy	$3.46 \times 10^4$ Joules
Repetition Rate	0.5 Hz

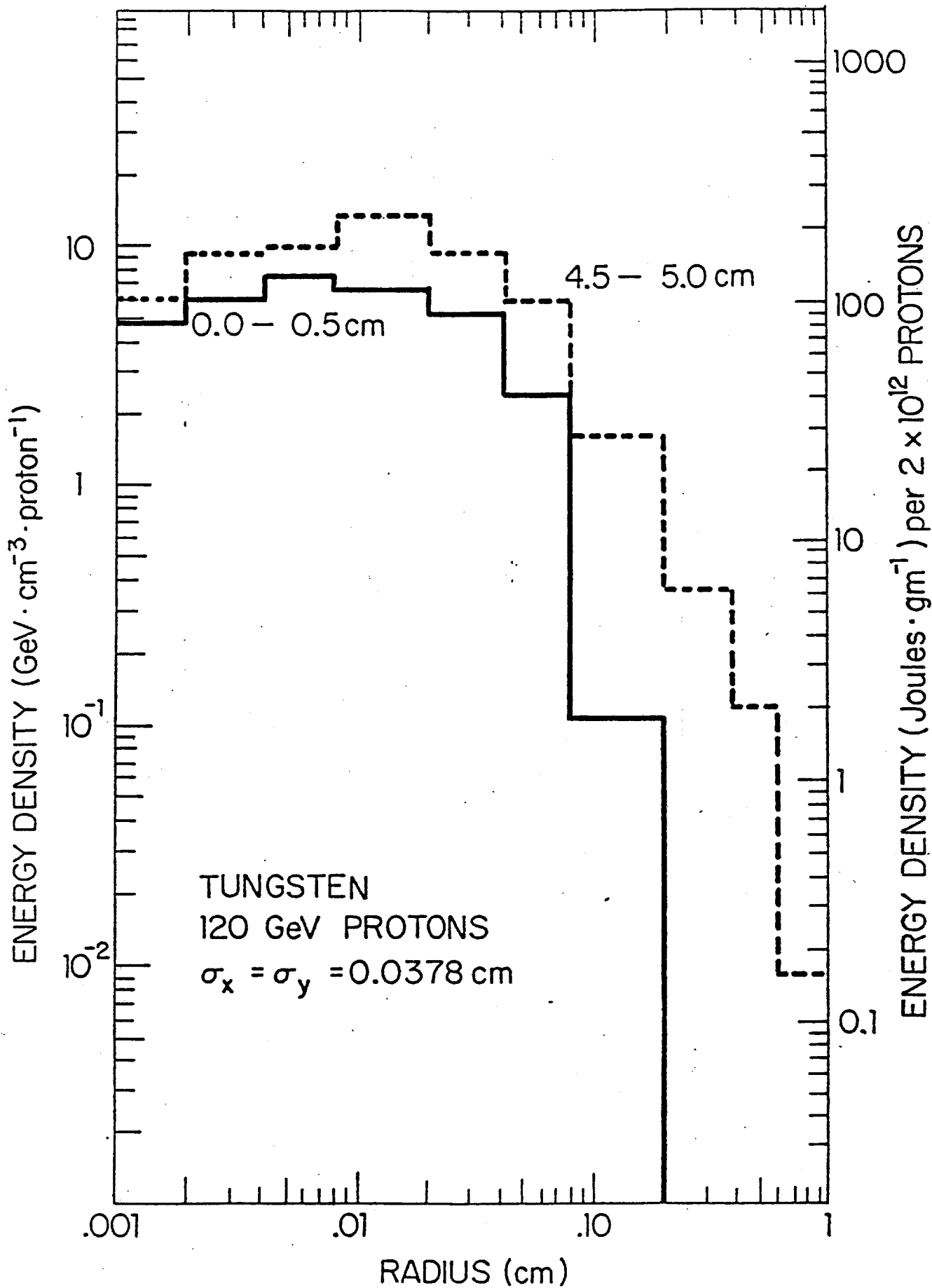


Figure 3-4

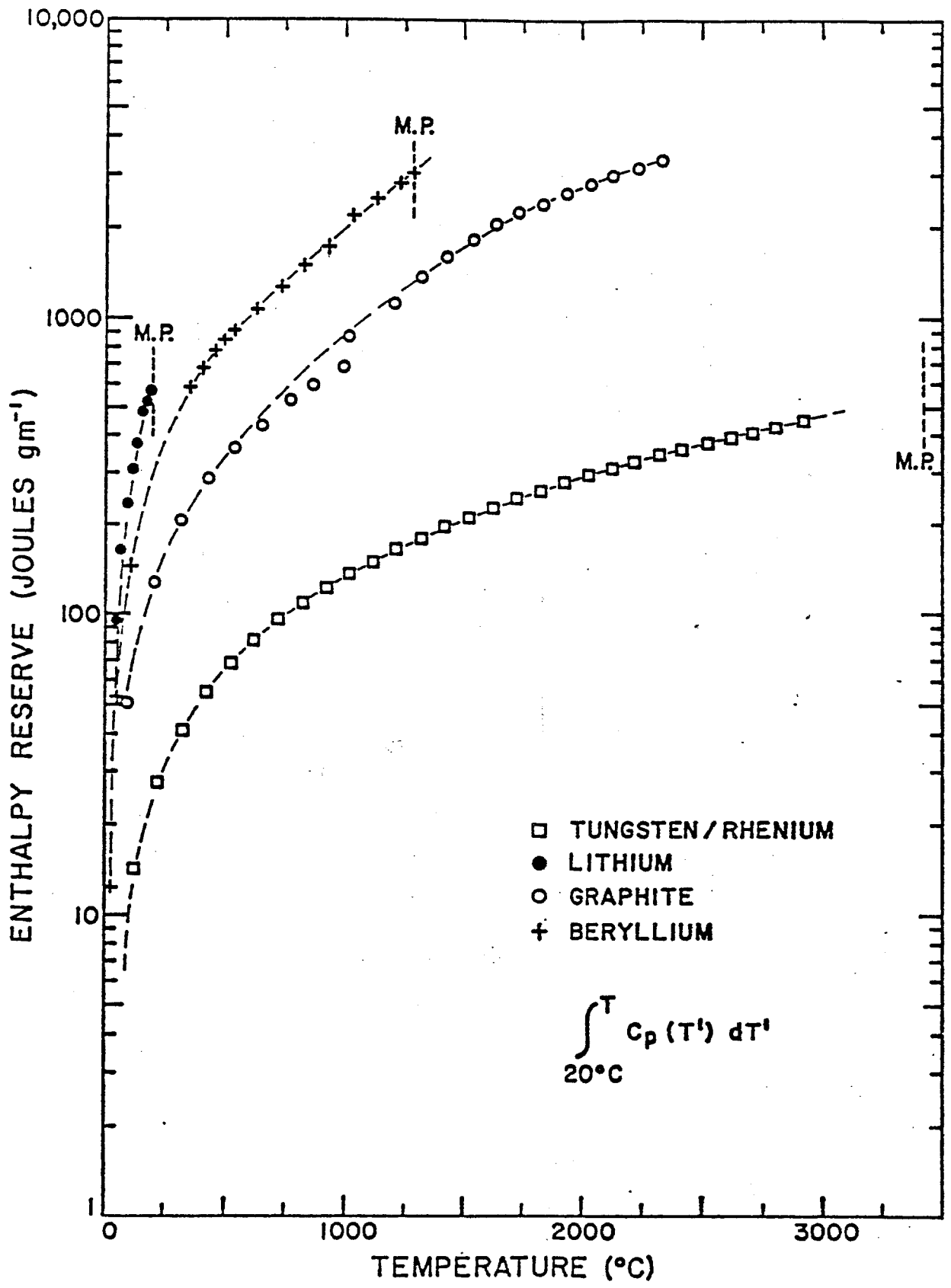


Figure 3-5

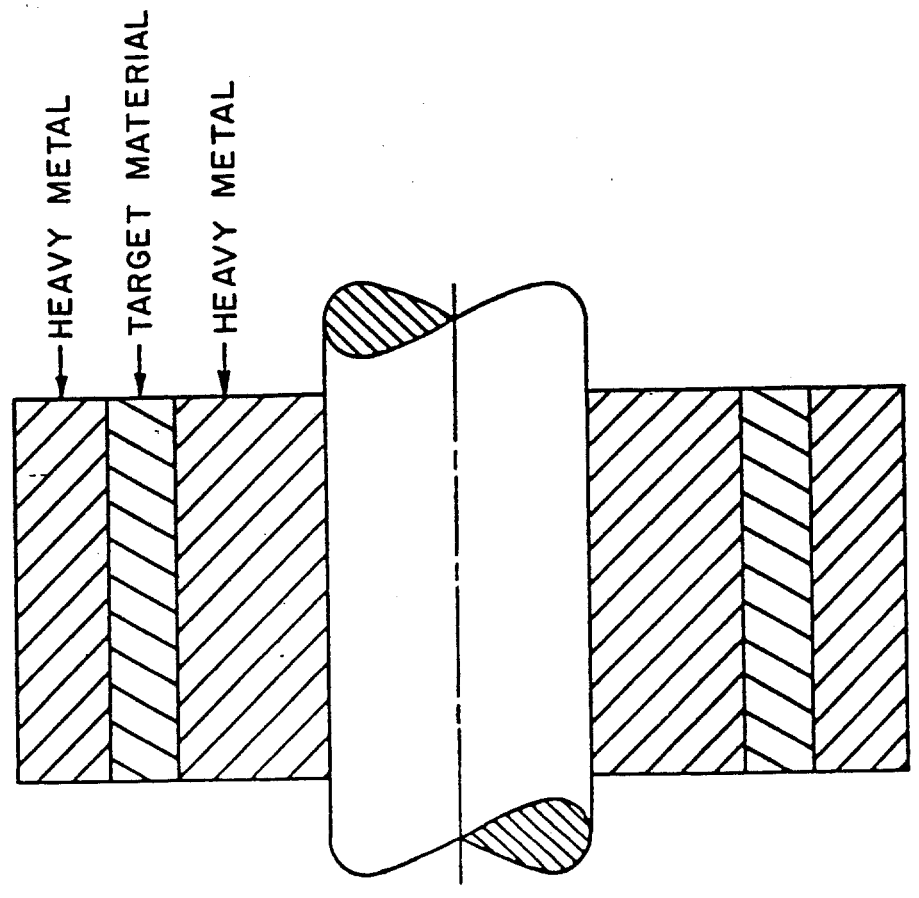
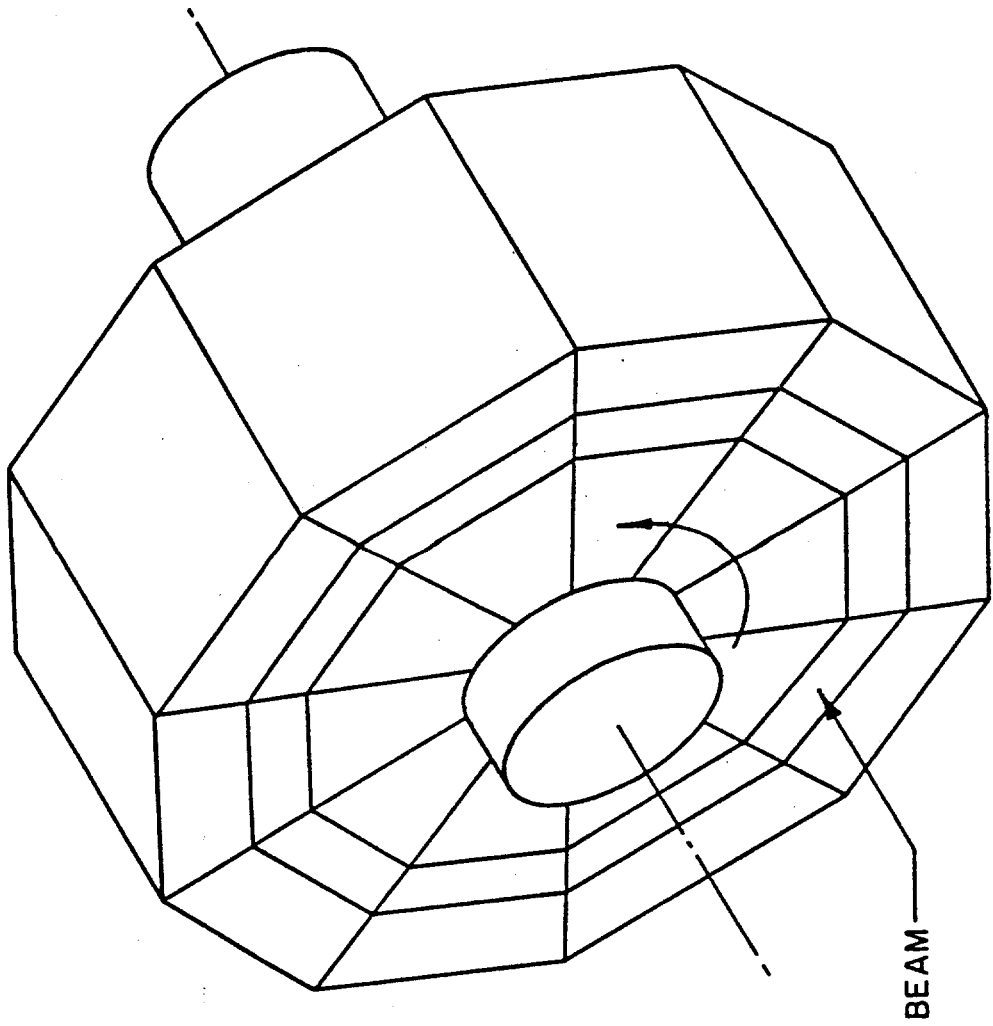


Figure 16

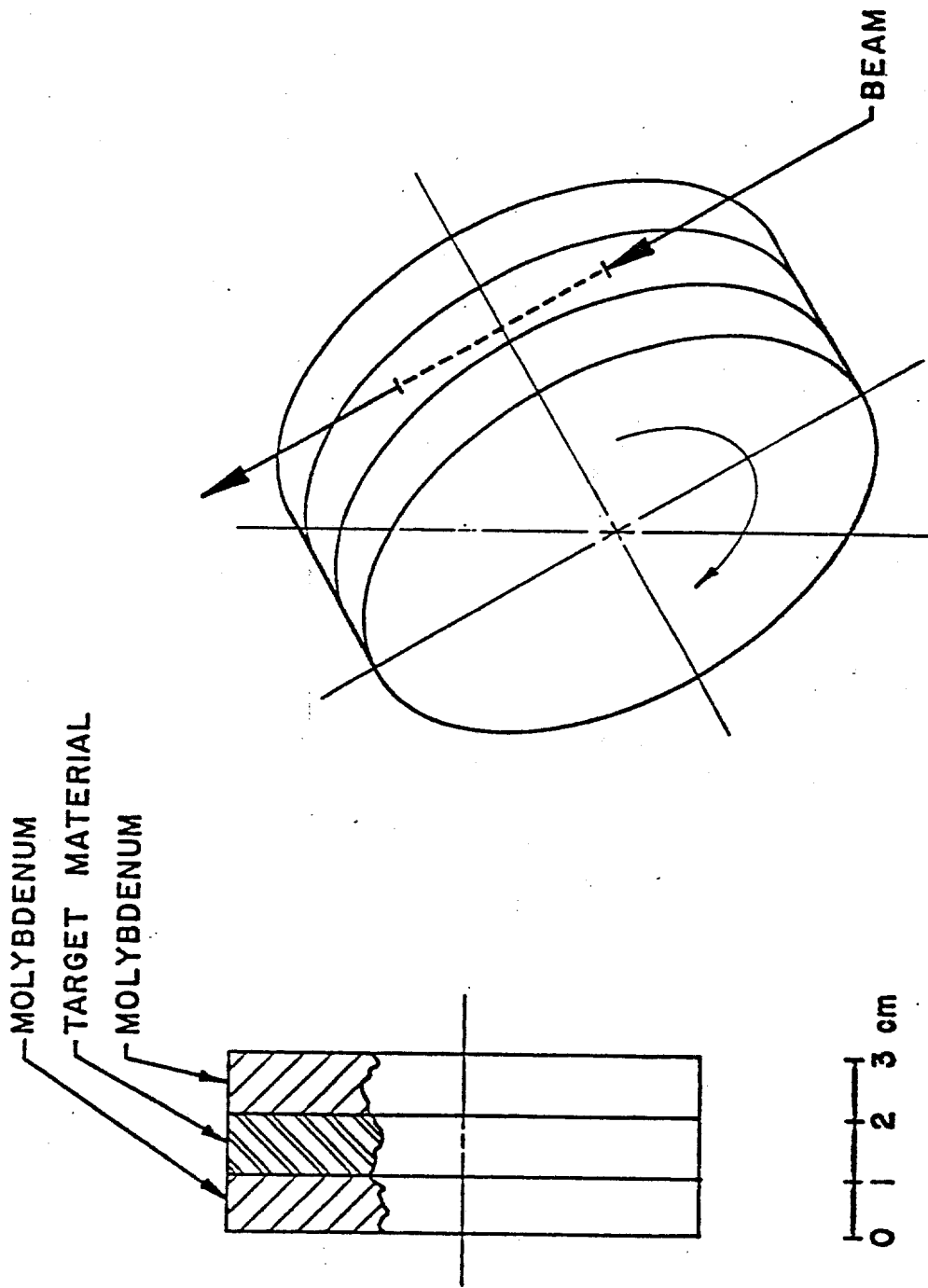


Figure 3-7

Beam Pulse Duration	$1.6 \times 10^{-6}$ sec
Energy Deposited/proton	1.26 GeV ( $1.81 \times 10^{-10}$ Joules)
Energy Deposited/pulse	346 Joules
Power Deposited	173 Watts
Average Temperature	100°C
Beam Size ( $\sigma_x = \sigma_y$ )	0.038 cm
Peak Energy Density/proton	13.4 GeV/cm <sup>3</sup>
Peak Energy Density/pulse	200.0 Joules/gm
Peak Temperature Rise	<1500.0°C

CERN

Peak Energy Density <sup>+</sup>	>185 Joules/gm
Peak Temperature Rise	1500°C
Average Temperature	800°C

<sup>+</sup>This rhenium target has been used for some time with no failures.

3.2.2 Antiproton Collection; the Lithium Lens. A study has been made of the relative merits of  $\bar{p}$  collection schemes that utilize a lithium lens, a pulsed quadrupole multiplet, or a conventional quadrupole triplet.<sup>2</sup> Since it was found that the lithium lens is far more efficient for the collection of  $\bar{p}$ 's, this section concentrates on the lens. The other options that are discussed will be pursued if the lens development lags.

The basic physical principle of the lithium lens is that a uniformly distributed electric current in a cylindrical conductor produces an azimuthal magnetic field with a constant radial gradient. Charged beam particles traversing the length of such a conductor experience a force that focuses them toward the axis. Lithium is an appropriate material for such a focusing device because it is the least-dense solid conductor, thereby minimizing  $\bar{p}$  absorption and multiple scattering.<sup>3</sup> The lens under development uses a 15-cm long lithium cylinder of radius 1 cm and requires a current of 0.5 MA to produce the desired gradient of 1000 T/m. Joule heating caused by direct current in the lithium is prohibitively large, so a 0.6 msec full-width unipolar sine-like pulse of amplitude 0.5 MA will be applied every 2 sec. Each pulse will generate about 6000 Joules of heat and the problem of removing this heat dominates the mechanical design of the lens. It is desirable to keep the average temperature well below the 180°C melting point of lithium because the 1.5% volume expansion that occurs upon melting could shorten the lifetime of the lens. The magnetic induction H created by the pulsed current does not have a constant radial gradient, due to the skin effect. Fig. 3-8 shows the variation of  $H/H_{\max}$  during one pulse.<sup>7</sup>

Energy deposition in a lithium lens located 14.5 cm (one focal length) downstream of a 5-cm tungsten target was calculated using the program MAXIM. Contributions from secondaries emerging from the target as well as from non-interacting 120 GeV protons were included. The heating due to the beam was found to be small compared to Joule heating.<sup>8</sup>

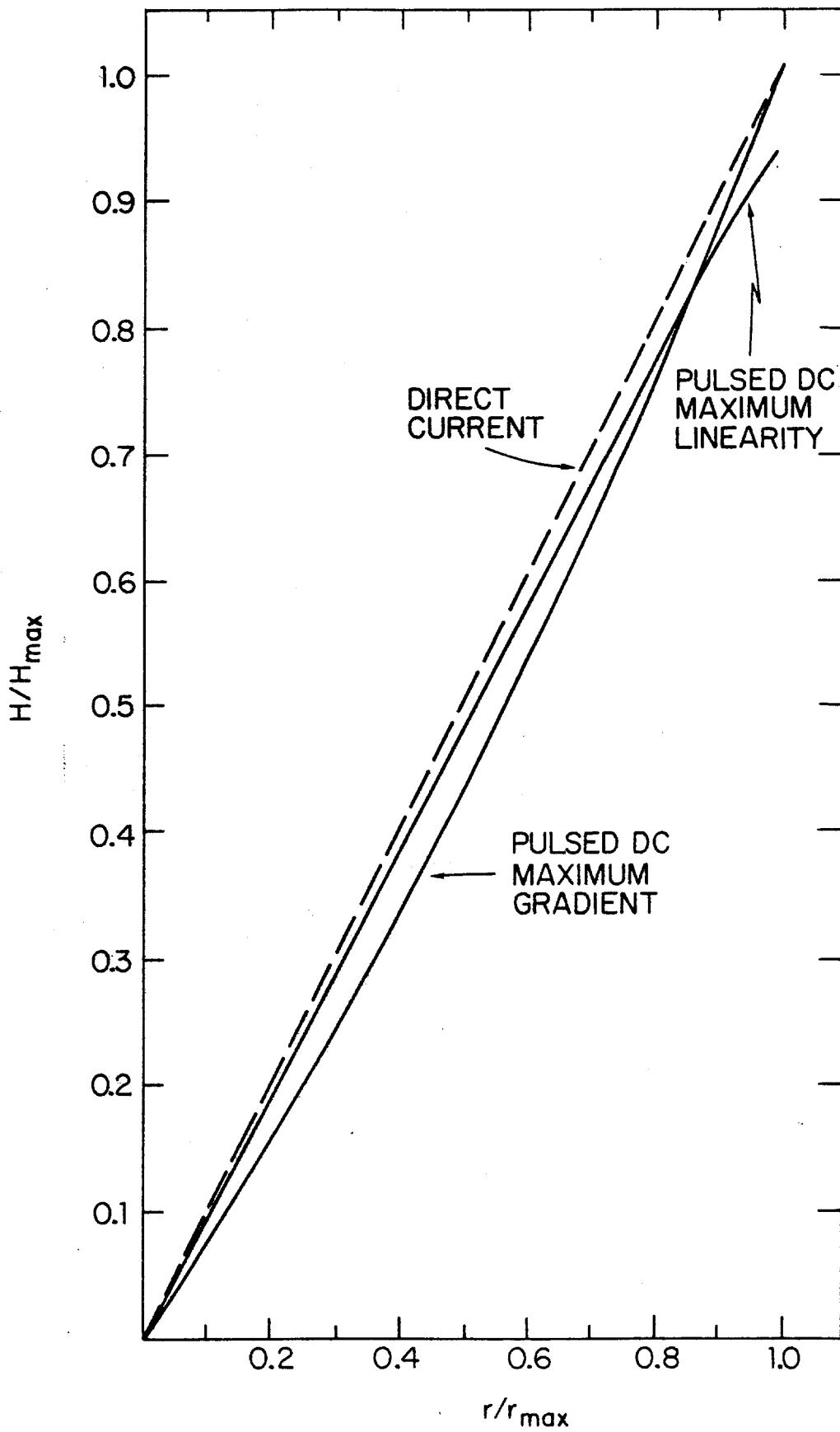


Figure 3-8

In case the lithium-lens development lags, linear and non-linear horns of the types developed for the CERN AA ring could be utilized. To optimize the  $\bar{p}$  rate, they require significantly longer targets. Preliminary results indicate that horns would not provide as good a collection efficiency as the proposed lithium lens at our  $\bar{p}$  energy. The larger currents required for the 8.89 GeV/c  $\bar{p}$ 's, as compared with 3.5 GeV/c at CERN, may make the horn construction very difficult. Another option would be to install a 5Q36 triplet.<sup>2</sup> This would limit the  $\bar{p}$  production system to small momentum spreads and emittances, but could be useful in the early stages of running.

3.2.3 Antiproton Selection. Downstream of the lithium lens, a pulsed dipole magnet will be used to select negative particles of energies near 8 GeV. Particles not selected, the remnants of the 120 GeV proton beam and other interaction products, continue towards the beam dump. The 8 GeV antiprotons pass through a channel in the beam dump and then into the transport line to the debuncher ring.

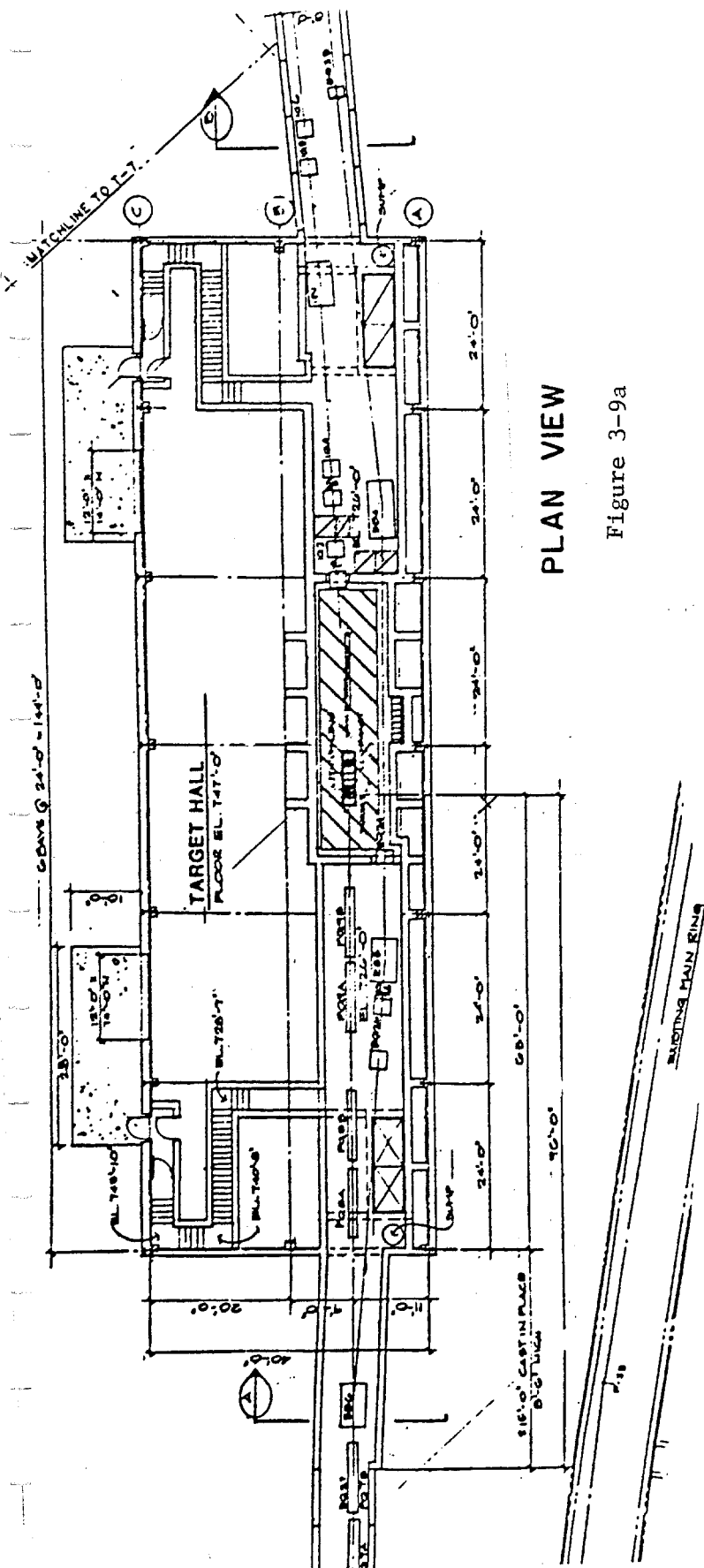
The pulsed magnet will be a dipole powered by a capacitive discharge supply similar to that of the lithium lens. The current pulse will be a half sine wave with  $\omega = 1200$  hz. The magnet aperture will be 3 x 3 cm, and the field integral will be 1.55 Tesla-meter. This will provide a 3° bend in the antiproton beam.

### 3.3 Target Hall

The antiproton production target, proton beam dump and the lithium lens for antiproton collection will be located in a vault downstream of the final quadrupole focusing system in the 120-GeV proton line. The dimensions of this vault are planned to be 7 ft by 33 ft with the floor located at 17 ft below grade, as shown in Fig. 3-9a, and 3-9b.

The upstream end of the hall is separated from the proton-beam transport tunnel by 3 ft of steel shielding. Further shielding is placed around the external walls of the vault in the earth. Below the vault two separate impermeable membranes are used to collect irradiated ground water. Shielding configurations that limit the irradiations of the soil and the above-ground fluxes to permissible values have been designed to allow operation at an intensity of  $10^{13}$  protons per second.

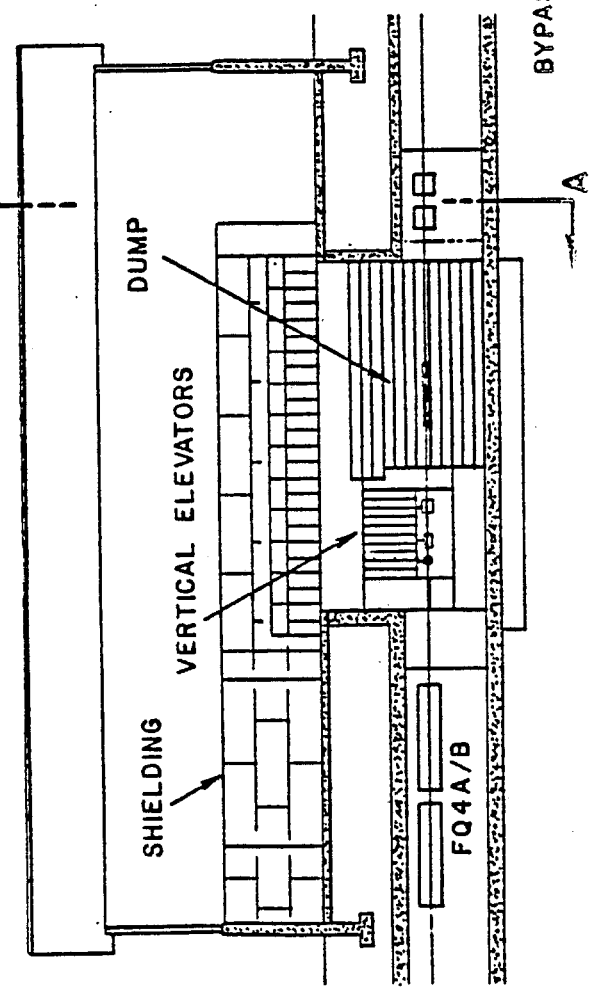
Downstream of the upstream end of the shield, within the target vault, a 3 ft high by 8 ft long and 2 ft wide volume of space is available for components. The space between this volume and the concrete walls and floors of the vault is filled with steel shielding. Access to the target station components is accomplished by raising one of a set of solid steel elevators into the Target Service Building. Each elevator segment extends 10 in. along the beam direction and 24 in. transverse to the beam. Each is 7 ft long in the vertical direction. The components are suspended from the bottom of the elevator. The 7 ft length makes it possible to place electronics and control systems immediately above each elevator segment without danger of radiation damage. An additional 3 ft of concrete is



PLAN VIEW

Figure 3-9a

ELEVATION



SECTION A-A

Figure 3-9b

required to keep the above-ground radiation levels within the Target Service Building below the maximum permissible level. Within the Target Service Building and surrounding the vault, a shielded area incorporating thick windows will be used to exchange elevator segments remotely. Work will be performed on components with remote manipulators. The manipulators will be used to exchange targets routinely. Access to the electronics at the top of the elevator segments will be possible when beam is not being delivered to the target station.

The last component in the beam before the dump is a pulsed magnet to bend the  $\bar{p}$ 's to the right by  $3^\circ$ , in order to separate them from the protons. The dump is a water-cooled graphite core 6 ft long surrounded by a steel jacket which fills the inside of the vault. The steel extends for 22 ft along the proton beam. The construction is similar to the dump developed for the Tevatron abort system.

Transport of the 8-GeV antiprotons to the Debuncher is discussed in Sec. 11.2.

References

1. "Calculation of Yields for the Fermilab Antiproton Source" Carlos Hojvat and A. Van Ginneken, Fermilab-Pub-82/43, 1982 (submitted to Nucl. Inst. Meth.)
2. E. Colton, "More on Antiproton Collectors,"  $\bar{p}$  note #120, Fermilab (unpublished).
3. B. F. Bayanov et al., "A Lithium Lens for Axially Symmetric Focusing of High Energy Particle Beams," Nuc. Inst. Meth., 1909(1981).
4. "MAXIM - Program to Simulate Cascades in Bulk Matter." A. Van Ginneken, Fermilab FN-272 (January 1975).
5. "High Intensity Targeting Workshop," Fermilab April 28-30, 1980.
6. F. Krienen and F. Mills, Spreading the Hot Spot on the Target,  $\bar{p}$  Note 70. E. Colton,  $\bar{p}$  Note 107.
7. "Skin Effect in Electrically Pulsed Cylindrical Conductors used as Focusing Devices," A.J. Lennox, Fermilab Report FN-379, January, 1983. "Optical Properties of Cylindrical Lenses," T.A. Vsevolozhskaya et al, Sov. Phys. Tech. Phys., Volume 20, No 12, 1556 (1976).
8. "Energy Deposition in the Lithium Lenses," A.J. Lennox,  $\bar{p}$  Note 204, Fermilab 1982 (unpublished).